Meteorol. Z. (Contrib. Atm. Sci.), PrePub DOI 10.1127/metz/2021/1107

Intercomparison and combination of low-cost urban air temperature measurement approaches

Lukas Meyer[1,2], Moritz Gubler[1,2,3*], Fred Meier[4] and Stefan Brönnimann[1,2]

[1]Oeschger Centre for Climate Change Research, University of Bern, Bern, Switzerland
[2]Institute of Geography, University of Bern, Bern, Switzerland
[3]Institute for Lower Secondary Education, Bern University of Teacher Education, Bern, Switzerland
[4]Chair of Climatology, Institute of Ecology, Technische Universität Berlin, Germany

(Manuscript received August 12, 2021; in revised form September 14, 2021; accepted October 14, 2021)

Abstract

Measurements of urban air temperatures (T_{air}) are vital to successful adaptation and mitigation policies to increasing urban heat stress. However, in-situ measurements in cities are often scarce and costly, and therefore low-cost approaches are increasingly used to study urban T_{air}. This allows for inexpensive, yet still highly spatially and temporally resolved observations of urban T_{air}. Despite their merits, a common issue of such low-cost approaches is lacking data quality and potential measurement errors. In this case study, we compare three low-cost measurement approaches regarding their ability to capture intra-urban variability of T_{air} over a period of 24 hours in Bern, Switzerland: a) A network of 79 low-cost measurement devices (LCD), b) bicycle mounted mobile measurements (BCY), and c) 581 Netatmo citizen weather stations (CWS). As the BCY sensor is actively ventilated, it is used as the reference for intercomparisons with LCD and CWS. Compared to the BCY, the median difference of T_{air} for LCD is found to be slightly negative over the entire study period (−0.08 K) as well as during night-time (−0.10 K), and positive during daytime (0.05 K). As the LCD are known to exhibit a positive bias during the daytime, the good agreement of BCY and LCD is speculated to indicate a positive daytime bias in BCY as well. The CWS show a positive median difference of 0.67 K over the entire study period, 0.98 K during night-time, and a negative difference of −0.23 K during daytime. It is hypothesized that these biases result from incorrect siting of the CWS by their owners installing CWS to close to buildings or walls. At night, these emit thermal radiation which could lead to the positive bias whilst the negative bias during daytime might result from buildings shading the CWS. BCY and LCD both show a distinct pattern of nocturnal intra-urban T_{air} variability, which is less pronounced in the CWS measurements. Furthermore, the intercomparison of the three approaches across local climate zones reveals that CWS do not well represent forested areas. Whilst the bias sources of the individual approaches require in-depth investigation in future studies (e.g., external heat sources and measurement height for BCY, daytime short-wave radiation errors for LCD, and nocturnal thermal heating by nearby buildings for CWS), we conclude that combining the three measurement approaches can allow to reduce the shortcomings of each approach regarding spatial and temporal resolution or correct biases inherent to one approach.

Keywords: Urban climate, Air temperature, Low-cost, Intercomparison, Citizen weather stations, Mobile measurements

1 Introduction

In the context of anthropogenic climate change, the risk of more intense, longer, and more frequent heat-waves is increasing (IPCC, 2021). In urban environments, this issue is further exacerbated by the urban heat island (*UHI*) effect, which, especially at night, leads to higher air temperatures (T_{air}) in cities compared to their rural surroundings (Howard, 1818; Sundborg, 1951; Oke, 1976; Stewart, 2011; Oke et al., 2017). This may result in an increase of heat-related health problems and mortality (Robine et al., 2008, Vicedo–Cabrera et al., 2021), and in a larger energy demand for cooling in summer (Frank, 2005) in areas where summers are hot enough that air conditioning is needed. Moreover, spatial patterns of intra-urban T_{air} and *UHI* intensity are subject to considerable variability (Stewart, 2011). Detailed knowledge about urban T_{air} variability is required to prevent negative impacts for vulnerable people such as people with lower socio-economic status (Sera et al., 2019) or elderly people (Gosling et al., 2009). Against the background of increasing urbanization (United Nations, 2019) and ongoing climate change (IPCC, 2021), a thorough understanding of the characteristics and spatiotemporal variability of urban T_{air} is therefore crucial for the development and implementation of adaption policies seeking to decrease heat-related risks in cities (IPCC, 2014; FOEN, 2018). Numeric urban climate models can provide such information, but they depend on observational data for evaluation and validation (Scherer et al., 2019). Data

*Corresponding author: Moritz Gubler, Universität Bern, Geographisches Institut, Hallerstrasse 12, 3012 Bern, Switzerland e-mail: moritz.gubler@giub.unibe.ch

from long-term observations (*LTOs*) are needed to evaluate general trends whilst intense observation periods (*IOPs*) can provide very high-resolution data to assess processes on the micro-scale, albeit for shorter periods.

However, meteorological measurement networks are often limited to rural environments to prevent urbanization effects in the data (WMO, 2006), and automated weather stations (*AWS*) are often subject to high instrumentation and maintenance costs (Grimmond, 2006; Chapman et al., 2015). In sum, this results in a general scarcity of high-resolution data on intra-urban variability of T_{air} (Muller et al., 2013), both of long-term observations and shorter-term but more intense observation phases.

One approach to circumvent these difficulties are mobile measurements with instrumentation mounted on vehicles such as bicycles. Bicycle mounted measurements (*BCY*) have proven to be a low-cost and reliable method to study the *UHI* (Melhuish and Pedder, 1998; Brandsma and Wolters, 2012) and to assess microclimatic variability in T_{air} due to changes in land surface type (e.g., cooling by forests or water surfaces; Rajkovich and Larsen, 2016). Bicycle transects can be particularly designed to the area of interest without having to install fixed weather stations, which provides flexibility regarding the study area. Due to their flexibility *BCY* measurements are well suited for *IOPs* (Scherer et al., 2019). Nevertheless, the usability of mobile measurement approaches may be restricted due to small sample size per measurement location, if not enough transects are carried out (Rajkovich and Larsen, 2016). Further limitations are uncertainty from time variation at different measurement sites and lack of spatial coverage due to only one transect being carried out at a time (Melhuish and Pedder, 1998). As a result, data from mobile measurements may be difficult to correctly interpret (Rajkovich and Larsen, 2016). One possibility to overcome these issues is the combination of mobile measurements with data from fixed measurement stations (Oke et al., 2017).

Recent advances in sensor technology and diminishing costs (Chapman et al., 2015) increasingly allow for the use of low-cost measurement devices (*LCD*) to study urban T_{air} (Gubler et al., 2021). Concerning urban T_{air} variability, a carefully deployed *LCD* measurement network may yield high-resolution data at low costs, whilst retaining the advantages of meaningful site selection, correct installation, and complete metadata (Gubler et al., 2021). Furthermore, such data could be used to complement other measurement approaches for urban T_{air} such as remote sensing (Voogt and Oke, 2003; White-Newsome et al., 2013), to develop and evaluate geostatistical models for *UHI* assessments (Burger et al., 2021), or to validate numerical urban climate model outputs (Chen et al., 2012). Finally, the combination of dedicated *LCD* networks with other low-cost observation approaches, such as crowd sourced data, could provide uniquely high observation density in urban areas. This large data availability might enable the application of new modelling techniques such as machine learning to map urban T_{air} (Zumwald et al., 2021) and generally allow for urban heat assessment at an increasingly small scale.

Besides these potentials, *LCD* measurements may be subject to considerable biases affecting data quality. Intercomparisons between *LCD* and standard meteorological measurement devices have shown varying biases depending on the type of sensor and radiation shield and depending on the selected observation period (Nakamura and Mahrt, 2005; Gubler et al., 2021). To reduce costs, *LCD* are often placed in passively ventilated radiation shields, leading to measurement biases during daytime especially at low wind speeds and high solar radiation. Nakamura and Mahrt (2005) found a mean daytime radiative error of 0.39 °C when comparing *LCD* measurements in passively ventilated multiplate radiation shields to *LCD* in actively ventilated shields. During the night, the error was smaller and slightly negative (−0.002 °C). Mauder et al. (2008) found mean differences of 0.42 °C between *LCD* in actively and passively ventilated radiation shields. Besides measurement biases, the maintenance effort of *LCD* measurement networks may be considerable, and therefore sustaining them over *LTOs* represents a substantial challenge (Chapman et al., 2015).

Crowd-sourced or citizen observation-based methods could overcome this challenge by offering the possibility to monitor the urban atmosphere with very high observation density at marginal costs or maintenance efforts (Muller et al., 2015). Additionally, the coverage of such data often concentrates in urban areas (Meier et al., 2017), which makes them ideal for urban heat studies, and their global availability provides opportunities for extending urban heat island studies to cities lacking dedicated measurement networks. Despite the considerable advantages of crowd-sourced approaches, the quality of such data remains a concern (Muller et al., 2015; Meier et al., 2017; Napoly et al., 2018). Bell et al. (2015) identified representativity errors as a source of uncertainty in citizen weather station measurements (*CWS*). Such errors can arise from improper siting or inadequate radiation shielding (Meier et al., 2017; Napoly et al., 2018; Cornes et al., 2020), which is further compounded by a lack of adequate metadata needed for bias corrections (Oke et al., 2017; Meier et al., 2017). To this end, quality controls and corrections for erroneous *CWS* data have been developed and tested (Meier et al., 2017; Napoly et al., 2018; Cornes et al., 2020). Nonetheless, previous research shows that T_{air} measured by *CWS* often exhibits a strong positive bias even after automated quality controls and bias correction when compared to official, automated weather stations. For instance, Napoly et al. (2018) found that single *CWS* showed T_{air} deviations of up to 4 K, whilst using spatial averages of *CWS* reduced the annual average mean hourly deviation to 0.95±0.41 K. In addition, Meier et al. (2017) report a positive deviation of 1.5 K between the spatial average of quality con-

trolled *CWS* T_{air} and that of reference stations during the night (24:00) in July 2015. However, these studies have focussed on *CWS* in large cities, such as Berlin, Toulouse, or Paris, with relatively homogenous topography and land use. Consequently, little evidence exists about the extent to which measurements from *CWS* can display intra-urban T_{air} variability in smaller-sized cities with heterogeneous topography and land use. If quality issues were reduced, *CWS* data could provide valuable high-resolution data as part of *LTOs* or *IOPs*.

The present case study aims to address limitations arising from low-cost measurement approaches of intra-urban T_{air} variability, by intercomparing the different approaches and investigating the different measurement biases inherent to each approach (*BCY*, *LCD*, and *CWS)*. To explore these biases, a statistical intercomparison of the three approaches is carried out for different daytimes and land use categories. Thereby, actively ventilated, high-resolution *BCY* measurements are used to validate measurements from a network of dedicated *LCD* and from publicly available, quality controlled measurements made by *CWS*.

Combining multiple low-cost approaches might not only allow to investigate biases inherent to a single approach, but also greatly increase overall observation density. This increased observation density was visualized by combining the three approaches on a map displaying the average nocturnal urban T_{air}.

2 Data and methods

2.1 Study area

All measurements were conducted within and around the city of Bern, Switzerland, (Fig. 1a) which is situated at an average altitude of 550 m a.s.l. Several hills (up to 947 m a.s.l.) directly surrounding the city and the prominent Aare River valley result in steep topographical gradients. (Fig. 1b). Bern has a population of about 140'000 people and a municipality area of 52 km^2, of which only 31.5 % are densely populated (HAFL, 2017). Summers in Bern are characterized by relatively high levels of precipitation (JJA monthly totals of about 110 mm) and monthly mean temperatures of about 17 °C (MeteoSwiss, 2020). The local climate of Bern is influenced by complex interactions of the surrounding local hills with meso-scale mountain and valley breezes. This causes relatively low wind speeds in the city and nocturnal cold air inflow from the mountains (Mathys et al., 2019).

2.2 Study period

The bicycle transects were conducted between the 7 August 2018, 05:49 and the 8 August 2018, 09:57 (local summertime CEST, UTC+2). Therefore, only *LCD*/*CWS* measurements made during this period are used for the analyses. This continuous 1-day measurement period was chosen to sample the whole diurnal cycle of urban T_{air} distribution and for personnel reasons, as a longer-term observation campaign sampling different times of day was not feasible.

The meteorological situation during the study period (Fig. 2) is derived from measurements at three *AWS* in and outside Bern. The first *AWS* (Bern/Zollikofen, hereafter ZOLL; 46.990744° N / 7.464061° E) is a station of the automatic monitoring network of the Swiss Federal Office of Meteorology and Climatology (MeteoSwiss) installed at 2 m above ground and lies within open fields in a rural area. The second *AWS* (Wankdorf, hereafter AFU; 46.96312° N / 7.46255° E) is operated by the city's administration for protection of the environment and air quality, is installed at 2.7 m above ground and lies within an urban area, surrounded by a school and a soccer stadium. The third *AWS* (Bollwerk, hereafter BOLL; 46.95096° N / 7.44045° E) is a rooftop station (24.6 m above street level) run by the Federal Laboratories for Materials Testing (EMPA) and lies within an urban area close to the main train station. Data from the *AWS* stations were obtained from the respective maintaining organisation.

The study period marked the end of a 9-day heatwave (Burger et al., 2021; Figs. 2a to 2d) and was not typical for high-*UHI* situations. During the study period T_{air} ranged from 17.9 °C to 31.7 °C at rural ZOLL, with slightly higher maxima at the urban reference stations (max. 32.1 °C; Fig. 2e). Wind speed peaked at 7 ms^{-1} around 22:00 on the 8 August (Fig. 2f), which was likely due to nearby thunderstorms. Solar irradiance was high throughout the day, with short drops due to clouds (Fig. 2g) and small amounts of precipitation (max. 1.5 $mm\,h^{-1}$) were measured at ZOLL in early morning (Fig. 2h).

2.3 Measurements

2.3.1 Low-cost devices

To assess the summertime variability of intra-urban T_{air}, a measurement network consisting of 79 *LCD* was installed within the greater area of Bern (Figs. 1a and 1b) between May and September 2018 (see Gubler et al., 2021 for a detailed description). A total of 73 *LCD* were placed within the city, whereas 6 *LCD* were located outside the city in rural environments. Locations were selected to be within a homogeneous microclimate (ca. 100 by 100 m) and representative of the local-scale land cover (Gubler et al., 2021). To circumvent vandalism, the *LCD* were placed at heights between 2.67 to 3.2 m above ground on free standing light posts, traffic signs, and similar poles (Fig. 3a). This is higher than 2 m standard height, but still within the acceptable range for urban T_{air} measurements (WMO, 2006). T_{air} was measured at 10-minute (min) intervals. The temperature sensors measure T_{air} with an accuracy of ±0.53 K between 0–50 °C (Table 1), with an *e*-folding time (or time constant) of 10 min needed to adjust to changes in surrounding T_{air} at airflow of 2 ms^{-1} (Onset Computer Corporation, 2018). Although the sensors were placed in

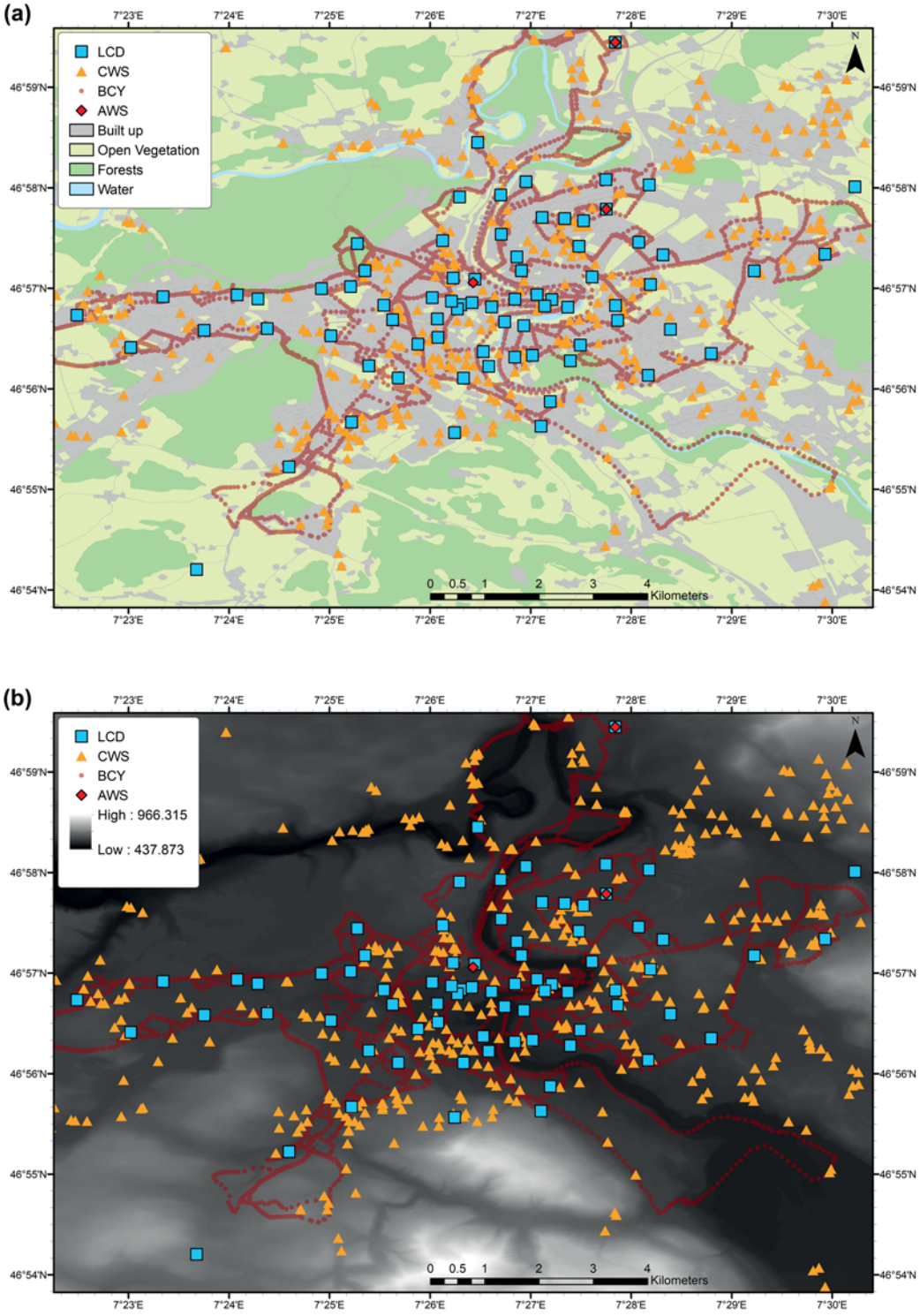

Figure 1: Overview over the study area showing the built-up city of Bern and its rural surroundings, overlaid with the measurement locations of the three different measurement approaches. The BCY transects (red circles), the LCD stations (blue squares), the Netatmo CWS (orange triangles), and the reference AWS (red diamonds) are shown. Background maps display (a) land use classes adapted from Urban Atlas (European Environmental Agency (EEA), 2012) and (b) topography (swissALTI3D; Federal Office of Topography (Swisstopo), 2017). Coordinates reference the World Geodetic System 1984 (WGS84).

passively ventilated radiation shields (Fig. 3d), the *LCD* measurements have been shown to be subject to radiative biases during daytime due to insufficient ventilation (Gubler et al., 2021). To illustrate, mean hourly differences from 16 May to 15 September 2018 (123 days) observed from parallel measurements between *LCD* and the three available *AWS* reference sites (ZOLL, AFU, BOLL) varied between 0.61 to 0.93 K (RMSE: 0.78 to 1.17 K) during daytime. Performance at night was substantially better, however, with mean summertime

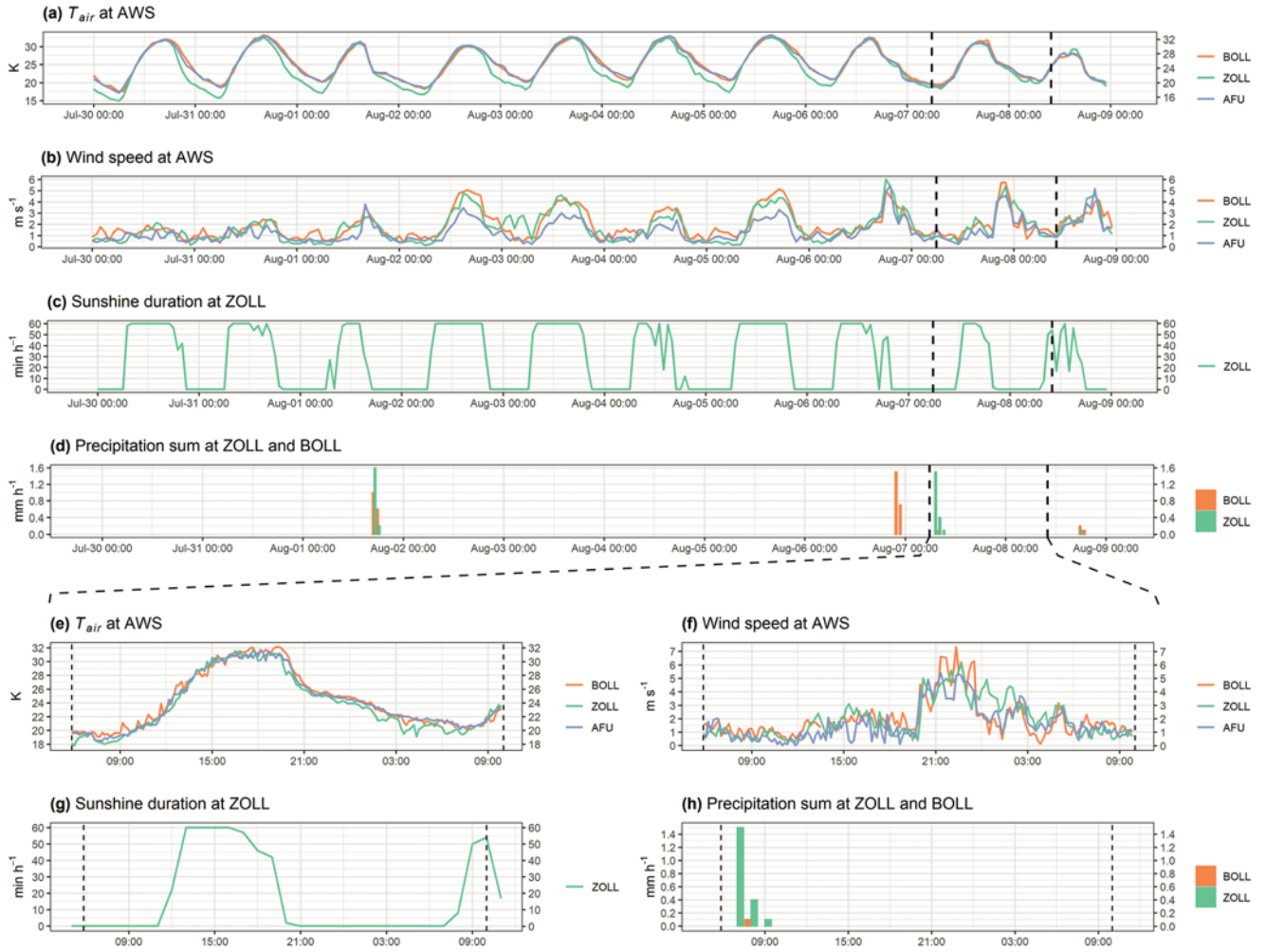

Figure 2: Atmospheric conditions during the 9-day heatwave from 30th July to 7 August measured at three professional AWS with (a) air temperature, (b) wind speed, (c) sunshine duration, and (d) precipitation. Dashed lines indicate the study period (7 August 2018, 05:49 to 8 August 2018, 09:57 CEST, UTC+2) with corresponding measurements of (e) air temperature, (f) wind speed, (g) sunshine duration, and (h) precipitation at the three AWS.

biases of −0.12 to 0.23 K (RMSE: 0.19 K to 0.34 K; Gubler et al., 2021). The *LCD* data used here were quality controlled by Gubler et al. (2021) for temporal consistency, errors from siting issues, physically implausible values, and potentially biased measurements during manual read out of the data, when the sensors were removed from the radiation shields and possibly exposed to short-wave radiation. Additionally, analysis of the T_{air} spread of each *LCD* showed that all data points within the study period fall within the physically plausible range defined as ±3.5 standard deviation of the entire *LCD* data throughout the study period (see appendix Figure S1).

2.3.2 Bicycle measurements

BCY measurements were conducted using a temperature sensor mounted to a bicycle at 0.8 m above ground (Fig. 3b), which is lower than recommended for urban T_{air} measurements (WMO, 2006) and could thus be prone to biases resulting from heat from vehicle exhausts, near surface inversions, or thermal radiation emitted from the surface. Studies investigating the urban T_{air} gradient close to the surface (Nakamura and Oke, 1988; Jansson et al., 2007) show that the near surface T_{air} can be up to 0.5 K higher than T_{air} at 2.5 m in built up areas. During the early afternoon hours these differences are largest and even exceed 0.5 K. However, in less well mixed regimes, such as urban parks after sunset, the near surface T_{air} can be around 1 K lower than T_{air} at 2.5 m. T_{air} was measured at 15 seconds (sec) intervals and mean inter point distance between subsequent measurements was 63.3 m. A 15 sec interval is lower frequency than in other similar studies, where a 1 sec interval is commonly used (Jansson et al., 2007; Brandsma and Wolters, 2012; Rajkovich and Larsen, 2016), but is sufficient to study the T_{air} variation in areas between the stationary measurements. A GPS continuously recorded the location of the bicycle. Three different approximately 2 hour long tran-

Figure 3: Illustration of the measurement set up (top row) and the measurement devices (bottom row) for the LCD (a & d), the BCY (b & e), and the CWS (c & f). Red ellipses highlight the location of the measurement device (Photo credits: M. Burger (a), M. Gubler (b), E. Lundstad (c) and (f), P. Duschletta (d), L. Meyer (e)).

Table 1: Technical details of the low-cost measurement devices according to Sensirion (2014a; 2014b), Meier et al. (2017), Büchau (2018), and Onset Computer Corporation (2018).

Network	Sensor Type	Ventilation	Accuracy	Resolution	*e*-folding time (time constant)	Manufacturer
Low-cost measurement device	Hobo Pendant 8k	Passive	±0.53 K (0–50 °C)	0.14 K	10 min (airflow 2 ms^{-1})	Onset Computer, Bourne MA, USA
Bicycle mounted sensor	Sensirion SHT21	Active	±0.3 K (25 °C)	0.01 K	5 to 30 sec	SENSIRION AG, Staefa ZH, Switzerland
Netatmo citizen weather stations	Sensirion SHT20	None (in unventilated aluminium cylinder)	±0.3 K (−40–65 °C)	0.04 K	approx. 25 min	SENSIRION AG, Staefa ZH, Switzerland

sects, covering a north-south cross section trough Bern, the eastern part of the city, and the west of Bern, were carried out repeatedly during the study period for a total of 14 transects (Figs. 1a and 1b; appendix Figure S4). To change drivers between transects, each transect started and ended at the Institute of Geography of the University of Bern (46.95283° N / 7.43540° E). Despite delay due to traffic and navigation errors, the transects were mostly initiated around the full hour. The temperature sensor has an accuracy of ±0.3 K, an *e*-folding time (time constant) of 5 to 30 sec (Sensirion, 2014b; Table 1), and was actively ventilated by a small computer fan (ventilation speed 11520 RPM and airflow rate 634 l min^{-1}; Micronel, 2003) placed within the same type of radiation shield as used for the *LCD* measurements (Fig. 3e). Due to its active ventilation and subsequently presumed low radiative error (Nakamura and Mahrt, 2005; Mauder et al., 2008), and high accuracy, resolution, and low sensor *e*-folding time, the *BCY* was used as a moving reference station to intercompare with *LCD*/*CWS*. The bicycle data were quality controlled as follows: Entries of 8 or more equal temperature values in a row were removed

as these are highly unlikely without logger malfunction. Any measurements made when the GPS had contact to 4 or less satellites were discarded, as their position is unreliable. Physically implausible measurements exceeding ±3.5 standard deviation of the entire data set were also removed. Moreover, to minimize any biases from vehicle exhausts when the bicycle was standing or moving slowly in traffic, data points below 9 m spatial distance to the previous datapoint, which corresponds to a velocity of 0.6 ms^{-1}, were removed. The quality control of *BCY* removed 1488 measurement points (21.96 % of entire data set), which were mostly due to low velocity of the bicycle (flagged 1178 data points), logger malfunctions leading to equal temperature values over multiple timesteps (flagged 260 data points), or number of satellites being 4 or less (flagged 302 data points). Note that one data point can be flagged by multiple quality control mechanisms.

2.3.3 Netatmo citizen weather stations

CWS from the Netatmo company are privately owned weather stations used to monitor atmospheric conditions outside and inside the owners' houses and usually consist of an outdoor and indoor module. The data set used here consists of hourly T_{air} measurements (instantaneous values) taken by the outdoor module (Figs. 3c and 3f). There exist 581 Netatmo *CWS* within the study area (Figs. 1a and 1b). A complete documentation of data retrieval is provided by Meier et al. (2017). Netatmo *CWS* do not measure at the same time, and therefore previous studies have assigned the measurements to the closest full hour (Napoly et al., 2018). Since this study focusses on relatively short time intervals, the original timestamps were kept and not assigned to the closest full hour. Therefore, every Netatmo station has slightly different measurement times of ±10 min around the full hour. The T_{air} sensor of *CWS* has an accuracy of ±0.3 K (Sensirion, 2014a; Table 1; Meier et al., 2017). Büchau (2018) found an *e*-folding time of approximately 25 min for Netatmo *CWS* in climate chamber experiments under calm conditions. A year-long comparison at a field site in Berlin between a *CWS* and an *AWS* revealed mean hourly differences within ±0.5 K, except for the morning hours from 07:00 to 12:00, where the *CWS* exhibits a mean negative bias of up to −1.3 K. However, the great uncertainty in the quality of Netatmo data stems from the fact, that there is no guarantee that the outdoor module has been set up correctly, and corresponding metadata is often lacking (Meier et al., 2017). The raw data was quality controlled to level O1 following the procedure of Napoly et al. (2018). Thereby, among other steps, stations with identical coordinates are removed, a lapse rate approach is applied for altitude correction, and statistical outliers from the hourly air temperature distribution are detected. Finally, missing values for single timesteps are interpolated by averaging the measurements taken before and after the missing values.

2.4 Analysis

2.4.1 Spatiotemporal matching of measurements

The intercomparison between the mobile *BCY* measurements and the fixed *LCD*/*CWS* measurements requires a spatiotemporal matching of the different measurement locations. Thereby, *LCD*/*CWS* measurements in proximity to *BCY* measurements are aggregated and the mean *LCD*/*CWS* T_{air} is compared to the measurement of the corresponding *BCY*. Two aspects of proximity must hereby be considered: The spatial distance between measurement locations should be small, so that T_{air} differences arising from different measurement locations are minimized. Additionally, the temporal difference between the measurement times should be minimized, so that differences due to the diurnal cycle of T_{air} are reduced.

Regarding spatial matching, *LCD*/*CWS* measurements were sought to be compared to *BCY* measurements within the same spatial source area. This source area can be defined as an ellipse around the measurement, which changes shape depending on prevailing wind direction, wind speed, and local land cover (Stewart, 2011; Oke et al., 2017). One practical approach is to define circular radii or ellipses with the long axis parallel to the wind direction (Brandsma and Wolters, 2012; Rajkovich and Larsen, 2016). In this study, the source area is simply defined as a circular area around the measurement location and thus assuming horizontal spatial distance to be the main driver of temperature differences at small scales, irrespective of the land cover type. Stewart (2011) recommends that no more than a few hundred meters be considered a source area of a measurement. Therefore, *LCD*/*CWS* and *BCY* measurements are only compared if they were within a specific spatial distance, or radius, from each other. Based on values chosen in previous studies, various radii between 100 and 3000 m were selected. The smaller radii (<1000 m) correspond to Stewart's (2011) recommendation and to radii chosen in previous studies using *BCY* measurements (Brandsma and Wolters, 2012; Rajkovich and Larsen, 2016) and *LCD* measurements (Burger et al., 2021). Larger radii (>1000 m) were used in studies which investigated *CWS* measurements (Napoly et al., 2018). Concretely, the T_{air} difference (ΔT) between each of the *BCY* measurements and the *LCD*/*CWS* measurements was calculated by the inverse distance weighted (*IDW*) mean of T_{air} for all the *LCD*/*CWS* within the defined distance, or radius, of corresponding *BCY* measurement. Hereby, the following formula was used (applied for *CWS*, hence $\Delta T_{\boldsymbol{CWS},IDW-BCY}$):

$$\Delta T_{CWS,IDW-BCY} = \frac{\sum_{i=1}^{n} \frac{1}{d_{CWS,i}} T_{CWS,i}}{\sum_{i=1}^{n} \frac{1}{d_{CWS,i}}} - T_{BCY} \qquad (2.1)$$

where n is the number of *CWS* within the defined distance of the *BCY* measurements, $d_{CWS,i}$ is the distance of

a *CWS* measurement to the *BCY* measurement, $T_{CWS,i}$ is T_{air} measured by the corresponding *CWS*, and T_{BCY} is the T_{air} measured by the *BCY* sensor. The Netatmo *CWS* have shown a positive bias at night (Chapman et al., 2017; Meier et al., 2017). Therefore, the temperature difference based on the minimum *CWS* T_{air} ($\Delta T_{CWS,MIN-BCY}$) was also calculated:

$$\Delta T_{CWS,MIN-BCY} = \min\{T_{CWS,1}, \ldots, T_{CWS,i}\} - T_{\text{BCY}} \quad (2.2)$$

where $\min\{T_{CWS,1}, \ldots, T_{CWS,i}\}$ is the lowest measured temperature of all *CWS* within the defined distance and T_{BCY} is the T_{air} measured by the *BCY* sensor.

In addition to the spatial distance criteria outlined above, *BCY* and *LCD*/*CWS* measurement were also temporally matched. Hereby, *LCD*/*CWS* measurements which are within the spatial distance criterion of *BCY* measurements, should still only be compared if the difference in measurement times was within a certain threshold. *BCY* measurements were made every 15 sec and *LCD* measurements every 10 min and therefore differences in measurement time range from 0 to 300 sec. For *LCD*, 15, 60, and 300 sec were chosen as thresholds to test. *CWS* measurements were made approximately every hour and missing time steps occurred frequently. Thus, differences in measurement time range from 0 to 134276 sec (37.3 hours). However, most differences were within 3600 sec (1 hour) and the median of measurement time difference was 986 sec. Therefore, 300, 600, 900, 1800, and 3600 sec were chosen as thresholds to test. In some cases, a *BCY* measurement was taken exactly in between two *LCD*/*CWS* measurement times. In that case, the *LCD*/*CWS* measurement taken before the *BCY* measurement was matched.

Several combinations of spatial and temporal differences were tested and compared by looking at the variance of theΔT values ($Var\,\Delta T$) between each *LCD*/*CWS* and *BCY*, whereas low $Var\,\Delta T$ indicates better agreement. This allowed to depict the "optimal" spatial distance and maximum time difference, or in other words, the spatial and temporal source area, when comparing *BCY* to *LCD*/*CWS*.

2.4.2 Intercomparison of temperature measurements

The assumptions about low biases and high accuracy of the *BCY* formulated in chapter 2.3.2 are checked by comparing the *BCY* measurements with reference measurements from the official *AWS* ZOLL and AFU. Therefore, $\Delta T_{BCY-AWS}$ was calculated according to Eq. 2.1 in chapters 2.4.1 for radii of 200 m and 500 m, but without the inverse distance weighting, as only one *AWS* was located within the selected radii of *BCY* measurements. To assess the ability of *LCD*/*CWS* to reproduce urban T_{air} variability as measured by *BCY*, $\Delta T_{LCD/CWS-BCY}$ of the entire period (7 August, 05:49 to 8 August, 09:57, CEST), night-time (7 August, 22:00 to 8 August 06:00, CEST), and daytime (7 August, 10:00 to 18:00, CEST) were analysed separately.

Given that the *UHI* is most pronounced at night and that the *LCD* biases are markedly lower than during the daytime (Gubler et al., 2021), further analyses were carried out considering only night-time T_{air}. To evaluate measurement biases depending on different urban land surfaces, ΔT during night-time was studied across different *Local Climate Zones LCZs* (Stewart and Oke, 2012). Using a *LCZ* map of Bern, derived from the World Urban Database WUDAPT (Ching et al., 2018; Fig. 4) every *BCY* measurement, and thereby the *LCD*/*CWS* observations compared to that *BCY* measurement, was assigned to the corresponding *LCZ*. This somewhat simplified approach ignores the effect of any surrounding *LCZs* but is assumed to provide a sufficient approximation.

2.4.3 Map of mean night-time temperatures

To visualize the increased observation density and the spatial pattern of urban T_{air} shown by each approach, a map of mean night-time urban T_{air} was created. However, bicycle observations cannot directly display mean nocturnal temperatures, as they are rarely made at the same location more than once.

BCY measurements therefore provide information on T_{air} at the measured location for one point in time but lack any information on the development of T_{air} over time (usually cooling during the night). To overcome these temporal inconsistencies, we corrected the *BCY* measurements based on cooling rates observed at nearby fixed measurement stations, as recommended by Brandsma and Wolters (2012) and Stewart (2011). Here, the individual *BCY* observations were corrected for nocturnal cooling using the difference between the *IDW* mean T_{air} at the time of the *BCY* measurement and the *IDW* mean nocturnal T_{air} observed by *LCD* within 200 m (Eq. 2.3).

$$\bar{T}_{BCY,NIGHT,t} = T_{BCY,t} - \left(\frac{\sum_{i=1}^{n} \frac{1}{d_{LCD,t,i}} T_{LCD,t,i}}{\sum_{i=1}^{n} \frac{1}{d_{LCD,t,i}}} - \frac{\sum_{i=1}^{n} \frac{1}{d_{LCD,night,i}} \bar{T}_{LCD,night,i}}{\sum_{i=1}^{n} \frac{1}{d_{LCD,night,i}}} \right) \quad (2.3)$$

where $\bar{T}_{BCY,NIGHT,t}$ denotes the corrected mean nocturnal T_{air} of a *BCY* observation made at time t, whilst $T_{BCY,t}$ is the actual T_{air} measured by *BCY* at time t. The term inside the bracket corresponds to the correction for nocturnal cooling by the difference between current T_{air} and mean night-time T_{air} at *LCD* within 200 m distance from the *BCY*. It is divided into two terms: The left term in the bracket denotes the *IDW* mean T_{air} measured by *LCD* within 200 m of the *BCY* at time t, whilst the right term is the *IDW* mean of mean night-time T_{air} measured by *LCD* within 200 m of the *BCY*. Variables within the terms are defined as in Eq 2.1. To increase the sample size, *BCY* measurement points located at a distance between 200 m and 500 m from an *LCD* were considered.

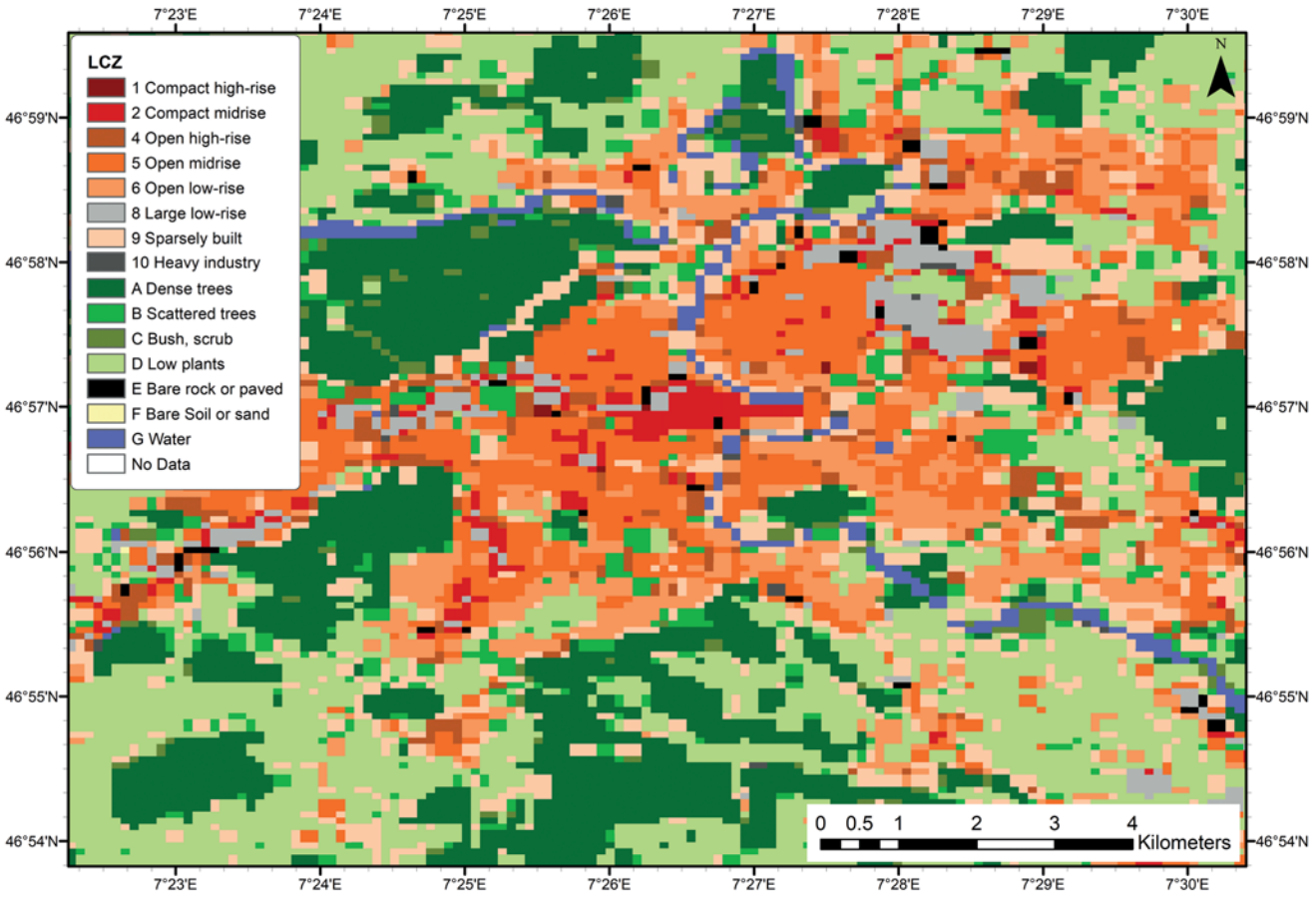

Figure 4: The Local Climate Zones in Bern as derived from the World Urban Database (Ching et al., 2018).

These measurements were corrected for nocturnal cooling by interpolating the *IDW* corrections from the closest *BCY* measurement backwards and forwards in time to which a correction was applied. The quality of this correction can be assessed in areas which were passed by the *BCY* multiple times at different stages of the night and were therefore corrected for nocturnal cooling multiple times separately. If the correction worked well, the mean night-time *BCY* T_{air} should be similar in these areas. *BCY* measurements not within 500 m of a *LCD* were not used for the analysis and map of mean night-time T_{air}.

3 Results

3.1 Spatiotemporal matching of measurements

Assessments of $Var\,\Delta T$ for different *BCY* source area distances and maximal time difference between *BCY* and *LCD*/*CWS* (Fig. 5) revealed that *LCD* generally have much lower $Var\,\Delta T$ (0.619 K^2) than *CWS* (1.849 K^2 for $\Delta T_{CWS,IDW-BCY}$ and 2.555 K^2 for $\Delta T_{CWS,MIN-BCY}$) and hence agree better with the *BCY* measurements.

Additionally, the criteria of time difference did not change $Var\,\Delta T$ substantially (Fig. 5), especially above source area radius of 1000 m (not shown). Within 1000 m, considering only *LCD* measurements made within 15 s of *BCY*, reduced $Var\,\Delta T_{LCD,IDW-BCY}$ by 0.100 K^2 compared to measurements made within 300 sec. The largest difference is observed when considering *LCD* measurements within 400 m of *BCY*, where $Var\,\Delta T_{LCD,IDW-BCY}$ is reduced by 0.336 K^2 if only measurements made within 15 sec are considered. For *CWS* the difference between the highest (3600 sec; equal to no time difference criteria) and the lowest (300 sec) time difference is 0.066 K^2 for $Var\,\Delta T_{CWS,IDW-BCY}$ and −0.062 K^2 for $Var\,\Delta T_{CWS,MIN-BCY}$, which means that using only *CWS* observations made closer in time to the *BCY* observations can increases $Var\,\Delta T$.

Concerning spatial source area, $Var\,\Delta T_{LCD,IDW-BCY}$ is lowest at a source area of 200 m (0.503 K^2) and increases with source area radius, whilst $Var\,\Delta T_{CWS,IDW-BCY}$ is highest at 200 m (2.286 K^2) and decreases with higher radii. $Var\,\Delta T_{CWS,MIN-BCY}$ does not change much relative to the radius and remains above 2 K^2.

For further analyses, *LCD* values within 200 m distance and with 300 sec maximal time difference and *CWS* values within 500 m distance and 3600 sec maximal time difference were used (Fig. 5). For *LCD*, a source area of 200 m provides low $Var\,\Delta T$ (0.563 K^2) and enough observations within the radius (35.2 % of

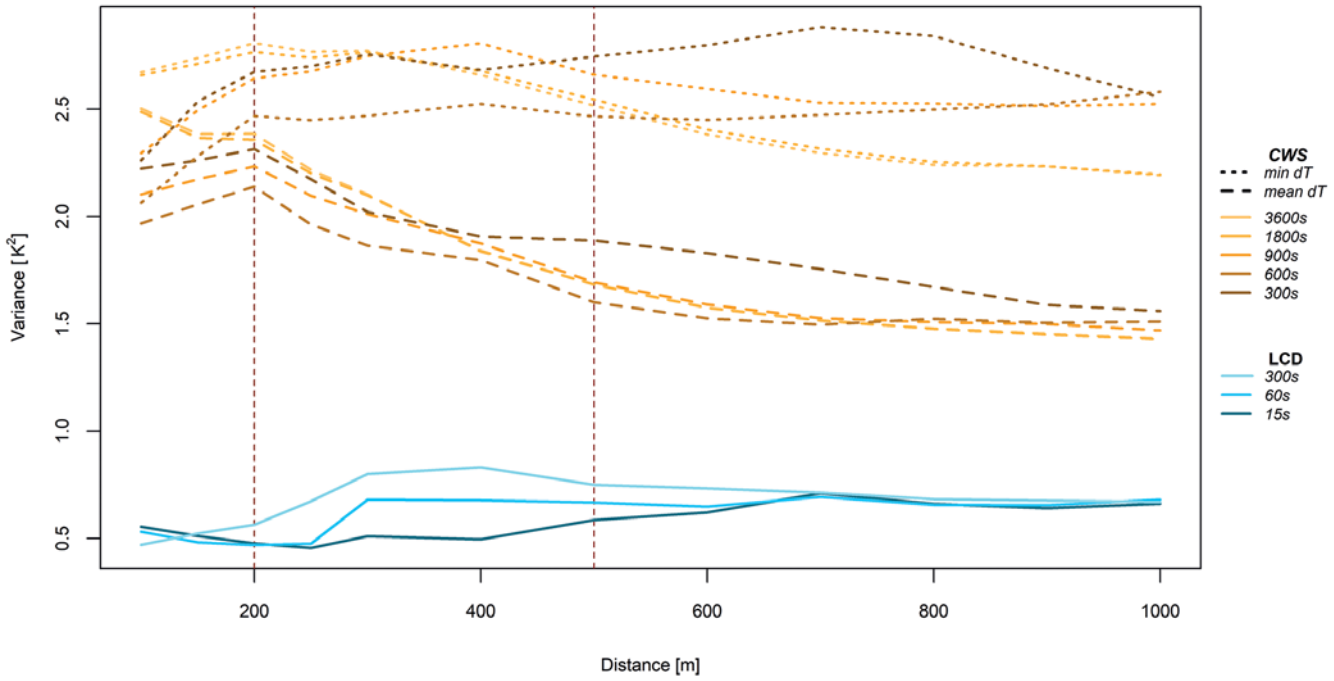

Figure 5: The variance of ΔT for different comparison methods for CWS (orange-brown lines; dotted lines is $\Delta T_{CWS,MIN-BCY}$, dashed lines is $\Delta T_{CWS,IDW-BCY}$) and for LCD (blue lines) for distances from 100 m to 1000 m and for different time differences indicated by colour shades. Vertical dashed red lines at 200 m and 500 m correspond to the "optimal" distances selected for further analyses for LCD/CWS, respectively.

BCY observations fall within 200 m of *LCD*, compared to only 14.4 % for 100 m). For *CWS* higher distances would slightly decrease *Var* Δ*T* but also average out spatial variability of T_{air} due to Bern's relatively small spatial extent and heterogeneous land use as well as topography.

3.2 Intercomparison of temperature measurements

The comparison between *BCY* and the *AWS* ZOLL and AFU revealed mean positive deviations (warm biases) of the *BCY*. At ZOLL mean Δ*T* is 0.50 K and 0.69 K for *BCY* measurements within 200 m (n = 32) and 500 m (n = 75) respectively. The increase of Δ*T* at a radius of 500 m can be explained by the larger amount of *BCY* measurements made over built-up and sealed surfaces compared to radius 200 m, where mainly *BCY* measurements made over the open field surrounding ZOLL are considered. The largest deviations, between 1.70 and 1.91 K, were recorded at midday around 12:50 on the 7 August, otherwise deviations never exceeded 0.86 K. Δ*T* at the urban station AFU was 0.41 K and 0.40 K for *BCY* measurements within 200 m (n = 27) and 500 m (n = 103) respectively. The largest deviations (0.83 to 1.9 K) were recorded in the early afternoon of the 7 August around 14:40 and to a lesser extent the morning around 06:43 of the 8 August), where deviations between 0.31 and 0.81 K occurred. Excluding daytime data (10:00 to 18:00), when largest deviations occurred, reduces the mean Δ*T* at ZOLL to 0.37 K and 0.50 K for 200 m (n = 29) and 500 m (n = 64) respectively and to 0.26 K and 0.23 K for 200 m (n = 19) and 500 m (n = 75) at AFU.

Concerning the differences between *BCY* and *LCD*/*CWS*, the analysis of Δ*T* for the whole period, night-time, and daytime (Fig. 6a) shows that the *LCD* agree better with *BCY* than *CWS*. Over the entire study period the median $\Delta T_{LCD,IDW-BCY}$ is −0.08 K with values ranging from −3.15 K to 5.15 K (*Var* Δ*T* 0.56 K^2). During night-time, the median Δ*T* is −0.10 K and the range is strongly reduced to −2.16 K to 1.50 K (*Var* Δ*T* 0.20 K^2), and during daytime *LCD* show a small positive difference (median $\Delta T_{LCD,IDW-BCY}$ 0.05).

$\Delta T_{CWS,IDW-BCY}$ is positive for the whole period (median 0.67 K) with a large range (−3.58 K to 9.31 K; *Var* Δ*T* 1.68 K^2). During night-time, $\Delta T_{CWS,IDW-BCY}$ is larger and positive (median 0.98 K) and the range is smaller (*Var* Δ*T* 1.06 K^2), whilst during daytime the median is −0.23 K.

$\Delta T_{CWS,MIN-BCY}$ is negative (median −0.37 K) for the whole period, with a range of −4.53 K to 7.35 K (*Var* Δ*T* 2.52 K^2). During night-time, the range is lower (*Var* Δ*T* 1.27 K^2) and the median is 0.01 K, indicating that using only the lowest *CWS* T_{air} within the source area reduces the positive bias observed in the *IDW* values. However, large positive Δ*T* of up to 5.28 K remain, and during daytime $\Delta T_{CWS,MIN-BCY}$

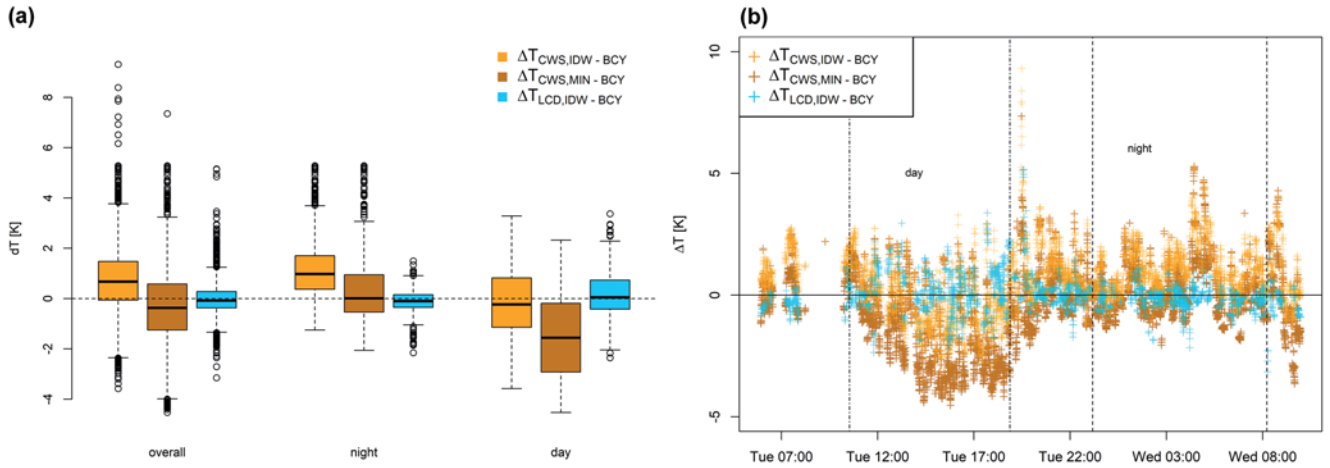

Figure 6: (a) Boxplots for ΔT between BCY and the following three approaches: inverse distance weighted mean temperature of CWS ($\Delta T_{CWS,IDW-BCY}$), minimum filtered temperature of CWS ($\Delta T_{CWS,MIN-BCY}$), inverse distance weighted mean temperature of LCD ($\Delta T_{LCD,IDW-BCY}$). (b) ΔT of every BCY – LCD/CWS comparison over the whole period. Vertical dashed lines indicate night-time and vertical dashed-dotted lines indicate daytime.

becomes strongly negative (median −1.56 K) showing that using only the lowest *CWS* T_{air} value underestimates T_{air} measured by *BCY*. The timeseries of ΔT (Fig. 6b) shows the low $\Delta T_{LCD,IDW-BCY}$, especially during night-time as well as the generally negative $\Delta T_{CWS,MIN-BCY}$ and $\Delta T_{CWS,IDW-BCY}$ during daytime and positive $\Delta T_{CWS,IDW-BCY}$ during night-time.

Evaluation of single large positive ΔT above 2.5 K for *LCD* ($n = 15$) show that 10 such values occurred when the *BCY* measured along the cool Aare River and compared T_{air} to *LCD* within the warmer old town and 5 occurred after the *BCY* exited a cool forest and compared T_{air} to an *LCD* within built-up residential areas. Single large negative ΔT below −2 K for *LCD* ($n = 9$) occurred after the *BCY* left a densely built area and entered a forest ($n = 5$), where an *LCD* displayed much lower T_{air}, between *BCY* measurements made on an open urban road and *LCD* within an avenue of trees ($n = 2$), and between *BCY* entering an urban park and the *LCD* within the park ($n = 2$). Evaluation of single large positive ΔT above 5 K for *CWS* ($n = 19$) shows that 11 occurred when comparing *BCY* values along the Aare to warmer urban *CWS*, whilst 8 come from *BCY* measurements made on a main road between a forest and industrial area compared to urban *CWS*. Single large negative ΔT below −3 K for *CWS* ($n = 4$) are found on a busy road over a city bridge ($n = 3$) and in a sub-urban area surrounded by open vegetation ($n = 1$), both occurring in the afternoon (14:20 and 15:20 CEST respectively).

Concerning ΔT by *LCZs*, *LCD* (Fig. 7a) showed low and similar ΔT for all *LCZs*, with few individual larger deviations. The mean of the median ΔT of all *LCZs* is −0.071 K, whilst the variance of the median ΔT of all *LCZs* is 0.033 K with a maximum positive ΔT of 1.50 K in *LCZ* B (scattered trees) and a minimum negative ΔT of −2.16 K in *LCZ* A (dense trees). Average sample size by *LCZ* was 43 and largest ($n = 215$) in *LCZ* 5 (open midrise), smallest ($n = 2$) in *LCZ* 10 (heavy industry), and zero in *LCZs* 1 and C (compact high-rise and bush, scrub). *CWS* (Fig. 7b) show positive biases for all *LCZs* (mean of the median ΔT of all *LCZs* is 1.01 K) with the exception of a negative bias (median ΔT is −0.60 K) for *LCZ* 1 (compact high-rise, $n = 2$) and larger positive biases for *LCZs* A (dense trees, $n = 116$) and C (bush, scrub, $n = 2$) with median ΔT of 2.12 K and 2.38 K respectively. The range of ΔT is greater than for *LCD* with a variance of the median ΔT of all *LCZs* of 0.48 K and a maximum positive ΔT of 5.28 K in *LCZ* 5 (open midrise) and a minimum negative ΔT of −1.25 K in *LCZ* D (low plants). Except for *LCZ* C (bush, scrub, $n = 2$) and 1 (compact high-rise, $n = 2$), all *LCZs* have single positive ΔT values exceeding 3 K. Average sample size by *LCZ* was 110 and largest ($n = 502$) in *LCZ* 5 (open midrise) and smallest in *LCZ* 10 (heavy industry, $n = 5$), and *LCZs* 1 and C (compact high-rise, $n = 2$; bush, scrub, $n = 2$).

3.3 Map of mean night-time temperatures

The map of mean night-time temperatures (Fig. 8a) shows the large observation density achieved by combining the three low-cost measurement approaches. The average distance between observation points (nearest neighbour) is 618 m for *LCD* only ($n = 77$), 198 m for *CWS* only ($n = 521$; out of the 581 *CWS*, 60 were missing T_{air} entries during night-time) and 195 m for *LCD* and *CWS* combined ($n = 598$), 37 m for *BCY* only ($n = 1329$), and 72 m for all three approaches combined ($n = 1907$). Generally, observation density is high in built-up areas and lower in open or vegetated areas, and the addition of *CWS* and *BCY* to the

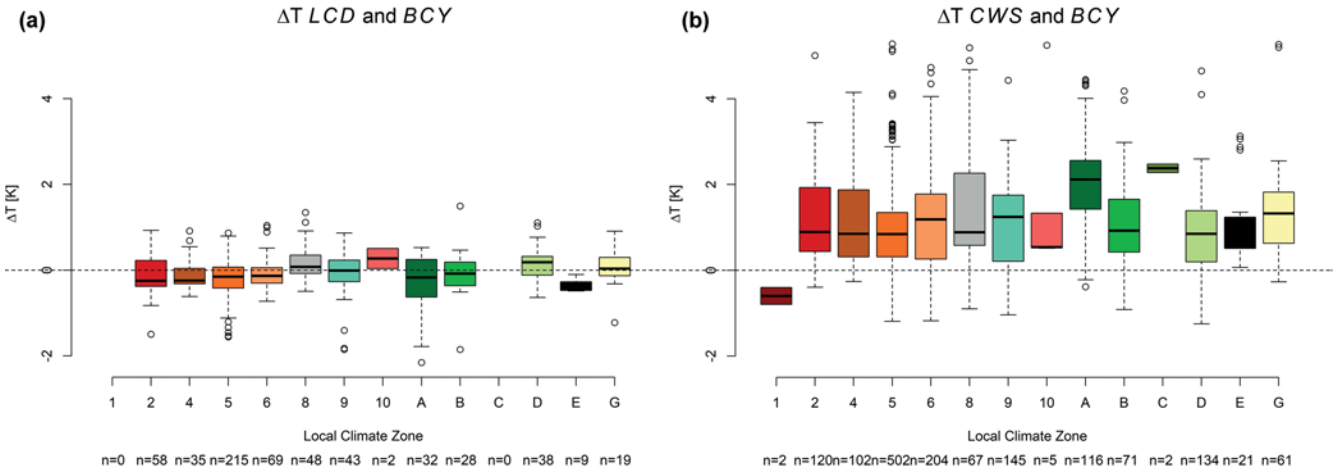

Figure 7: ΔT by LCZ for (a) the LCD measurements and (b) the Netatmo CWS during night-time (22:00 to 06:00, CEST). The number n at the bottom of each plot shows the number of measurements within a class.

Table 2: Distribution of nocturnal (22:00 to 06:00, CEST) T_{air} from the three measurement approaches.

Measurement approach	5th percentile	50th percentile	95th percentile
BCY	21.0 °C	22.6 °C	23.7 °C
LCD	21.1 °C	22.7 °C	23.7 °C
CWS	22.2 °C	23.7 °C	25.7 °C

dedicated *LCD* network further increases the observation density within built-up areas. The *BCY* measurements often cover transitional areas between distinct surface types, e.g., changes in Tair between urban areas and forests, urban parks, or the Aare River. The *CWS* extend the observed area into the sub-urban areas around Bern, which are not covered by either *LCD* or *BCY*. The average lapse rate is $-0.005\,\mathrm{K\,m^{-1}}$ for *BCY*, $-0.009\,\mathrm{K\,m^{-1}}$ for *LCD*, and $-0.006\,\mathrm{K\ m^{-1}}$ for *CWS* (appendix Figure S2). The distribution of nocturnal T_{air} (Table 2) was very similar for *LCD* and *BCY*, whilst *CWS* exhibited a far larger range and higher median.

Concerning the spatial T_{air} distribution, the *BCY* and *LCD* (Fig. 8c) clearly show the increased temperatures in the city centre and densely built-up areas (T_{air} between 22.5 and 24 °C), with a marked drop towards sub-urban and rural areas (T_{air} between 20 and 21.5 °C, with a few cases reaching 22.5 °C).

This pattern is far less clear in the *CWS* (Fig. 8b). Whilst the *CWS* display more stations with high T_{air} in the urban centre, and lower T_{air} with increasing distance from the centre, there are still many *CWS* which measured high T_{air} outside of the urban areas. This leads to a lessened T_{air} contrast between urban and sub-urban or rural areas in *CWS*: 61 *CWS* stations recorded values above 25 °C, of which only 17 were within the old town and city centre and 44 in the surrounding city, suburbs, or even rural villages. 7 *CWS*, none of which were within the city centre, recorded values above 27.5 °C. Furthermore, whilst *LCD* and especially *BCY* capture the cooling effect of vegetated areas (Fig. 8c) or the Aare River, the *CWS* for the most part fail to depict these cooler areas.

Finally, areas which were visited by the *BCY* more than once and were corrected for nocturnal cooling multiple times, show very similar mean night-time T_{air}, in most cases differing only by 0.5 to 1 K. Only on two such occasions, does T_{air} differ by more than 2 K, one of which fell onto a border of a forest and urban area and the other in a sub-urb (appendix, Figure S3).

4 Discussion

4.1 Definition of bicycle source area

T_{air} differences between single *BCY* observations and spatially aggregated *LCD*/*CWS* measurements within various spatial and temporal distance of the *BCY* observations (Fig. 5) were evaluated. The analysis showed that *LCD* measurements agree well with *BCY* measurements within a radius of 200 m ($Var\,\Delta T$ $0.56\,\mathrm{K^2}$), whilst *CWS* show larger differences ($Var\,\Delta T$ $1.68\,\mathrm{K^2}$) and depend on aggregation within a larger area or radius (500 m). These radii confirm the findings of Brandsma and Wolters (2012), who used linear regression to predict urban air temperature as measured from a bicycle using surface characteristics. They found that surface characteristics within the local scale (radius $\leq$ 400 m) have a larger influence on air temperature than micro-scale (radius $\leq$ 50 m). However, in a city with heterogeneous topography and relatively small spatial scale as Bern, the 500 m chosen for *CWS* might still violate the criterion that "*field sites be representative of local-scale surroundings*" (Stewart, 2011; p. 107).

The increase of $Var\,\Delta T$ in *CWS* observations made closer in time to the *BCY* observations could be related

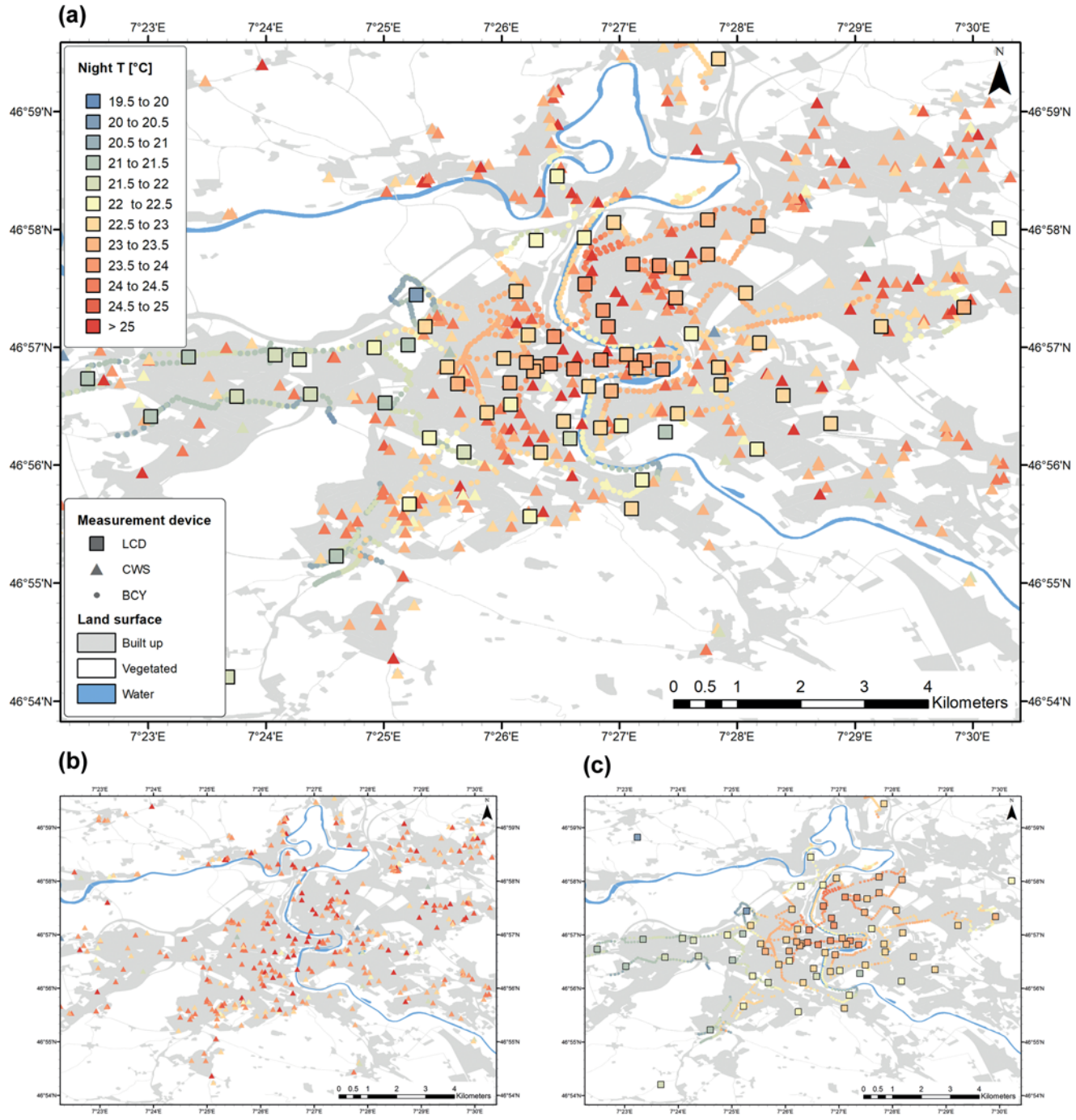

Figure 8: (a): Map of mean night-time (22:00 to 06:00, CEST) temperatures from all three measurement approaches: LCD (squares), CWS (triangles), and BCY (circles). (b): Same as (a) but with only the CWS. (c): Same as (a) but with only the LCD and BCY. Land surface based on the Urban Atlas (European Environmental Agency (EEA), 2012).

to the high *e*-folding time (approximately 25 min) of the Netatmo *CWS* observed by Büchau (2018). This effect is largest for *BCY* measurements made close in time to the *CWS* measurement and could thereby cause larger differences between *BCY* and *CWS* measurements. At spatial distances below 200 m, where the source area is often close to identical, the temporal distance does not influence $Var\,\Delta T$ of *LCD*. However, as spatial distance increases (200 m to 500 m) and source area of *BCY* and *LCD* differ more, using only *LCD* measurements made close in time to *BCY* reduces $Var\,\Delta T$. Nonetheless, the low differences in $Var\,\Delta T$ for different time distance criteria shows that *BCY* (or other) T_{air} measurements made at high temporal (sub minute) resolution can be well compared to less highly resolved measurements up to hourly measurement intervals.

However, as the single high ΔT discovered between *BCY* and *LCD* measuring different source areas (urban park vs. urban area or Aare River vs. old town) highlight, biases arise from the circular source area definition. When not explicitly deployed to observe these transition areas, where large T_{air} gradients are expected, further studies using *BCY* measurements could vary the *BCY* source area depending on the homogeneity of surrounding *LCZs* or only compare *BCY* and stationary measurements made within matching and homogeneous source areas. Additionally, elliptical source areas with the long axis parallel to the predominant synoptic wind conditions measured at nearby professional weather might be used (Rajkovich and Larsen, 2016).

4.2 Analysis of ΔT and bias source evaluation of low-cost approaches

The warm bias of the *BCY* compared the official reference stations ZOLL and AFU might be explained by the relatively low sensor height of *BCY* of 0.8 m compared to 2 m above ground for the reference stations, as well as the difference in measured surface type, which is sealed, dark asphalt roads for *BCY* and an open field for ZOLL and a small urban park for AFU. Thereby, heat from vehicle exhausts or thermal radiation from the surface could cause a positive bias in the *BCY* measurements (Nakamura and Oke, 1988; Jansson et al., 2007; Oke et al., 2017). Consequently, future *BCY* measurements should measure T_{air} at 2 m standard height. These considerations raise the point, that any upcoming claims on biases (both of *LCD* and *CWS*) must be viewed cautiously, since the *BCY* measurement's own biases were only superficially explored and not fully addressed here. To circumvent this issue, we recommend that future studies using *BCY* measurements carry out direct comparison measurements with reference data from *AWS* over an extended period allowing to robustly quantify the biases.

Comparison of ΔT (Fig. 6) across three comparison methods ($\Delta T_{LCD,IDW-BCY}$, $\Delta T_{CWS,IDW-BCY}$, and $\Delta T_{CWS,MIN-BCY}$) revealed good agreement between *BCY* and *LCD*, with a median $\Delta T_{LCD,IDW-BCY}$ of −0.08 K. This is lower than ΔT observed by Gubler et al. (2021), who carried out parallel measurements between the same *LCD* network and professional *AWS*. They found mean positive ΔT of 0.4 K and 0.56 K for the entire summer of 2018 (16 May to 15 September) and hourly averaged ΔT between −0.6 K and 2.2 K during the 9-day heatwave prior to the study period. This could be explained by the positive bias found in the *BCY* measurements, thus reducing ΔT to *LCD*, which also exhibited a positive bias (Gubler et al., 2021).

The comparison between *BCY* and *IDW CWS*, however, revealed large ΔT for the whole study period (median $\Delta T_{CWS,IDW-BCY}$ 0.67 K) with an increased positive bias during night-time (median 0.98 K) and small negative bias during daytime (−0.23 K). Similar biases were also found by Meier et al. (2017) and Napoly et al. (2018) and were hypothesized to stem from incorrect siting of the *CWS* by their owners, potentially installing the *CWS* to close to buildings or walls, which, especially during the night, emit thermal radiation. Furthermore, such proximity to walls or complete sheltering leads to a lower sky-view factor of the *CWS* and thus reduced longwave radiative cooling. Finally, heating of houses or reduced air flow close to buildings could lead to less cooling at night. The negative bias during daytime could again be explained by proximity to buildings, leading to shading of the *CWS*. The absence of a positive bias during daytime further supports the findings of Napoly et al. (2018) who suggested that the quality control they applied to the *CWS* has for the most part removed *CWS* data with shortwave radiation errors. Overall, assigning and quantifying the biases observed in *CWS* is challenging due to the lack of documentation or metadata available for each station.

Compared to the *IDW CWS* values, using only the minimum *CWS* T_{air} within the *BCY* source area, reduced the positive bias during the night-time (median 0.01 K) but led to a strong negative bias (median −1.56 K) during daytime. This indicates that applying simple minimum filtering techniques to *CWS* data might be used to reduce the observed positive bias during night-time, but this should be carefully evaluated in further intercomparisons between *CWS* and reliable weather stations. Nonetheless, averaging the values from multiple *CWS* gave more robust results, agreeing well with previous studies (Chapman et al., 2017; Meier et al., 2017; Napoly et al., 2018).

The analysis of ΔT by *LCZ* (Fig. 7) highlights the difficulties of *CWS* to represent T_{air} measured within forests (*LCZ A*), where median ΔT was 2.12 K. Moreover, it shows a uniform positive bias across *LCZs*, again indicating that *CWS* biases stem from microscale siting issues common to the majority of *CWS*, independent of surrounding local climate. However, the short study period and small sample size make clear statements difficult. Overall, the observed nocturnal biases in the *BCY* (between 0.24 K to 0.52 K, depending on the source area size and reference *AWS*) and *LCD* (−0.10 K) measurements are many times smaller than the variation in nocturnal T_{air} they display (the difference between the 5th and 95th percentile of T_{air} is 2.7 K for *BCY* and 2.6 K for *LCD*; see Table 2; Fig. 8). This means that the ratio of T_{air} signal to bias ranges from about 5:1 to 10:1 for *BCY* and is 1:26 for *LCD*, which still allows to display meaningful variation in T_{air}, as shown in the map of mean nocturnal air temperature (Fig. 8). This does not hold true for the *CWS* (bias 0.98 K with 3.5 K range between 5th and 95th percentile of T_{air}) where the ratio of air temperature signal to bias is around 1:3.5.

4.3 Potentials and limitations of the presented low-cost approaches

One major limitation and caveat of this study (and a difficulty of bicycle measurements in general) is the limited

temporal coverage and short study period (Rajkovich and Larsen, 2016). If bicycle observations are to be incorporated into longer term studies, dedicated campaigns are needed, such as carried out by Brandsma and Wolters (2012) who completed 183 transects within a 3-year period. This would allow for a more robust statistical analysis and allow to study differences between the measurement approaches across varying weather conditions, such as changes in windspeed or high solar irradiation.

Keeping this in mind, the approaches presented in this study complement each other well regarding spatial coverage (Fig. 8). Whilst the *LCD* are set up in representative areas or specific areas of interest, their limited number means that they cannot sample every neighbourhood. *CWS*, however, cover all populated areas including sub-urban neighbourhoods, whilst the *BCY* measurements provide information on changes in T_{air} whilst moving between the stationary measurements.

Concerning the observed spatial distribution of mean night-time temperatures, *BCY* and the *LCD* (Fig. 8c) clearly show intra-urban variability of T_{air} including higher nocturnal T_{air} in densely built-up urban areas and lower T_{air} in rural or vegetated areas. Overall, the spatial T_{air} distribution agrees with previous studies on the urban T_{air} of Bern (Burger et al., 2021; Gubler et al., 2021).

The Netatmo *CWS* show the general pattern of increased night-time T_{air} in urban areas with overall lower T_{air} away from the city centre, but single *CWS* with high T_{air} diminish the pattern: Out of the 61 *CWS* displaying unusually high T_{air} of above 25 °C, 44 were in sub-urban or rural areas. This further supports the argument made in Section 4.2, that *CWS* exhibit positive biases from microscale siting issues during night-time.

The cities where T_{air} from Netatmo *CWS* were studied (Chapman et al., 2017, Fenner et al., 2017; Napoly et al., 2018) are much larger and their land use and topography is more homogeneous than in Bern (e.g., London, Paris, Berlin). It seems that in small cities with a complex topography and perhaps generally, further measures are needed to increase the usability of Netatmo *CWS*. Future efforts could be directed towards developments of a quality control for single *CWS* with unreasonably high nocturnal T_{air}. A station-by-station assessment of *CWS* based on reference stations might identify and correct *CWS* with consistent large biases. Considering the low availability of professional *AWS* in urban environments, dedicated *LCD* networks might provide such reference data. Such a station-by-station correction is difficult however, since *CWS* are often spread throughout populated areas and can be at considerable distances to and in very different climatic environments than stationary reference stations. The flexibility of *BCY* measurements could bridge this gap, allowing repeated transects targeting specific single *CWS* or groups of *CWS* where the *BCY* could serve as reference data.

5 Conclusion

The goal of this work was to compare and show the potential of three different low-cost approaches for mapping the intra-urban variability of T_{air}: A dedicated network of *LCD*, *BCY* measurements and Netatmo *CWS*. The actively ventilated *BCY* measurements and the passively ventilated *LCD* were able to reproduce the general pattern of the night-time T_{air} distribution, with higher T_{air} in densely built-up areas. Compared to the *BCY*, the naturally ventilated *LCD* show a slight positive bias during daytime (median ΔT 0.05 K, $Var\,\Delta T$ 0.54 K^2), with better agreement during nighttime (median ΔT −0.10 K, $Var\,\Delta T$ 0.20 K^2). The *CWS* capture the general pattern of the nocturnal T_{air} differences between densely and less densely built-up areas, but not in the same magnitude and clarity as *BCY* and *LCD*, due to many high (>25 °C) mean night-time T_{air} observations in sub-urban and rural areas. This points to incorrect *CWS* set-up by the owners, highlighting the need for more complete metadata. The intra-urban variability of T_{air} is not well captured by *CWS*, especially the *LCZ* A (forest) was not properly reproduced, which is expected as *CWS* are usually not set up in forests by their owners. Spatially averaged values of T_{air} should be used in favour of single *CWS*, although the heterogeneity of land use and topography as well as the smaller spatial extent of Bern, makes averaging across large areas difficult. Further, quality control, stronger emphasis on metadata, or correction through reference stations would increase the applicability of *CWS* T_{air} measurements. More studies on *CWS* observations of the urban atmosphere in small cities with complex topography and heterogeneous *LCZ* distribution are needed to fully develop their potential. Generally, a more thorough understanding and definition of the *source area* of an urban measurement is recommended for future work, perhaps including land cover and wind speed and direction.

Overall, however, the presented combination of multiple low-cost approaches is regarded to wield large potential due to the unprecedented spatial and temporal resolution it offers at relatively low costs. This makes it well suited for measurements of the urban atmosphere in cities where professional *AWS* are not available at a spatial density required for intra-urban heat assessment. Furthermore, we showed that combining multiple approaches allows to reduce the shortcomings of each. *BCY* measurements, for example, allow to study areas not covered by stationary measurements, whilst the lower spatial and temporal coverage of *BCY* can be bridged by long term *LCD*/*CWS* networks. The higher biases observed in single *CWS* might be investigated or corrected using nearby *LCD* or by *BCY* observations specifically deployed for that purpose. Whilst further methodological improvements to each individual low-cost approach are promising, future urban climate studies within the low-cost paradigm should consider combining low-cost approaches such as the ones presented here.

Data availability

The data sets used for the analyses can be accessed and downloaded from: https://boris.unibe.ch/id/eprint/157253.

Acknowledgements

This work is dedicated to Hans Kallen, the former technician of the Geographical Institute of the University of Bern who passed away in late 2018. His technical support and advice were indispensable to the success of the measurement campaign. Furthermore, we thank all the contributors from the Climatology group of the University of Bern for conducting the bicycle transects, as well as the owners of the Netatmo *CWS* for providing their data to the public.

LM, MG, and SB designed the study. LM carried analysed the data, wrote, revised, and edited the original draft. MG, SB, and FM assisted with data analysis, commented on, and refined all versions of the manuscript.

Appendices

Supplementary figures (Figures S1 to S4) and the The *R* code used for the analyses in this study are in the supplement.

References

Bell, S., D. Cornford, L. Bastin, 2015: How good are citizen weather stations? Addressing a biased opinion. – Weather **70**, 75–84. DOI:10.1002/wea.2316.

Burger, M., M. Gubler, A. Heinimann, S. Brönnimann, 2021: Modelling the spatial pattern of heatwaves in the city of Bern using a land use regression approach. – Urban Climate **38**, 100885, DOI:10.1016/j.uclim.2021.100885.

Brandsma, T., D. Wolters, 2012: Measurement and Statistical Modeling of the Urban Heat Island of the City of Utrecht (the Netherlands). – J. Appl. Meteor. Climatol. **51**, 1046–1060. DOI:10.1175/JAMC-D-11-0206.1.

Büchau, Y.G., 2018: Modelling Shielded Temperature Sensors – An Assessment of the Netatmo Citizen Weather Station. – Master Thesis, Meteorological Institute Unversity of Hamburg, Hamburg.

Chapman, L., C.L. Muller, D.T. Young, E.L. Warren, C.S.B. Grimmond, X. -M. Cai, E.J.S. Ferranti, 2015: The Birmingham Urban Climate Laboratory: An Open Meteorological Test Bed and Challenges of the Smart City. – Bull. Amer. Meteor. Soc. **96**, 1545–1560. DOI:10.1175/BAMS-D-13-00193.1.

Chapman, L., C. Bell, S. Bell, 2017: Can the crowdsourcing data paradigm take atmospheric science to a new level? A case study of the urban heat island of London quantified using Netatmo weather stations: Crowdsourcing the London UHI. – Int. J. Climatol. **37**, 3597–3605. DOI:10.1002/joc.4940.

Chen, F., R. Bornstein., S. Grimmond, J. Li, X. Liang, A. Martilli, S. Miao, J. Voogt, Y. Wang, 2012: Research Priorities in Observing and Modeling Urban Weather and Climate. – Bull. Amer. Meteor. Soc. **93**, 1725–1728. DOI:10.1175/BAMS-D-11-00217.1.

Ching, J., G. Mills, B. Bechtel, L. See, J. Feddema, X. Wang, C. Ren, O. Brousse, A. Martilli, M. Neophytou, P. Mouzourides, I. Stewart, A. Hanna, E. Ng, M. Foley, P. Alexander, D. Aliaga, D. Niyogi, A. Shreevastava, P. Bhalachandran, V. Masson, J. Hidalgo, J. Fung, M. Andrade, A. Baklanov, W. Dai, G. Milcinski, M. Demuzere, N. Brunsell, M. Pesaresi, S. Miao, Q. Mu, F. Chen, N. Theeuwes, 2018: WUDAPT: An Urban Weather, Climate, and Environmental Modeling Infrastructure for the Anthropocene. – Bull. Amer. Meteor. Soc. **99**, 1907–1924. DOI:10.1175/BAMS-D-16-0236.1.

Cornes, R.C., M. Dirksen, R. Sluiter, 2020: Correcting citizen-science air temperature measurements across the Netherlands for short wave radiation bias. – Meteor. Appl. **27**, e1814. DOI:10.1002/met.1814.

European Environmental Agency (EEA), 2012: Copernicus Land Monitoring Service – Urban Atlas [data set], https://land.copernicus.eu/local/urban-atlas.

Federal Office of Topography, Swisstopo, 2017: High precision digital elevation model of Switzerland (swissALTI3D) and high precision building model of Switzerland (swissBUILDINGS3D 2.0) [data set]. – https://www.swisstopo.admin.ch/en/geodata/height/alti3d.html.

Fenner, D., F. Meier, B. Bechtel, M. Otto, D. Scherer, 2017: Intra and inter 'local climate zone' variability of air temperature as observed by crowdsourced citizen weather stations in Berlin, Germany. – Meteorol. Z. **26**, 525–547. DOI:10.1127/metz/2017/0861.

Fenner, D., A. Holtmann, F. Meier, I. Langer, D. Scherer, 2019: Contrasting changes of urban heat island intensity during hot weather episodes. – Env. Res. Lett. **14**, 124013. DOI:10.1088/1748-9326/ab506b.

FOEN, Federal Office for the Environment, 2018: Hitze in Städten. Grundlage für eine klimaangepasste Siedlungsentwicklung [EN: "Heat in cities: Foundations for climate adapted residential development"]. – Federal Office for the Environment, FOEN, Bern.

Frank, Th., 2005: Climate change impacts on building heating and cooling energy demand in Switzerland. – En. Build. **37**, 1175–1185. DOI:10.1016/j.enbuild.2005.06.019.

Gosling, S.N., J.A. Lowe, G.R. McGregor, M. Pelling, B.D. Malamud, 2009: Associations between elevated atmospheric temperature and human mortality: a critical review of the literature. – Climate Change **92**, 299–341. DOI:10.1007/s10584-008-9441-x.

Grimmond, C.S.B., 2006: Progress in measuring and observing the urban atmosphere. – Theor. Appl. Climatol. **84**, 3–22. DOI:10.1007/s00704-005-0140-5.

Gubler, M., A. Christen, J. Remund, S. Brönnimann, 2021: Evaluation and application of a low-cost measurement network to study intra-urban temperature differences during summer 2018 in Bern, Switzerland. – Urban Climate **37**, 100817. DOI:10.1016/j.uclim.2021.100817.

HAFL, 2017: Schlussbericht Urban Green & Climate Bern – Die Rolle und Bewirtschaftung von Bäumen in einer klimaangepassten Stadtentwicklung [EN: "Final report Urban Green & Climate Bern – the role and cultivation of trees in climate adapted urban development"]. – School of Agricultural, Forest and Food Sciences HAFL, Bern.

Hasenfratz, D., O. Saukh, C. Walser, C. Hueglin, M. Fierz, T. Arn, J. Beutel, L. Thiele, 2015: Deriving high-resolution urban air pollution maps using mobile sensor nodes. – Pervas. Mob. Comp. **16**, 268–285. DOI:10.1016/j.pmcj.2014.11.008.

Howard, L., 1818: The Climate of London, Vol. 1 – London.

IPCC, 2014: Climate Change 2014: Climate Change 2014: Impacts, Adaptation, and Vulnerability. Part A: Global and Sec-

toral Aspects. Contribution of Working Group II to the Fifth Assessment Report of the Intergovernmental Panel on Climate Change. – Cambridge University Press: New York, NY.

IPCC, 2021: Summary for Policymakers. In Climate Change 2021: The Physical Science Basis. Contribution of Working Group I to the Sixth Assessment Report of the Intergovernmental Panel on Climate Change. – Cambridge University Press. In Press.

Jansson, C., P.-E. Jansson, D. Gustafsson, 2007: Near Surface Climate in an Urban Vegetated Park and Its Surroundings. –Theor. Appl. Climatol. **89**, 185–193. DOI:10.1007/s00704-006-0259-z.

Mathys, H., R. Maurer, B. Messerli, H. Wanner, M. Winiger, 2019: Klima und Lufthygiene im Raum Bern. Resultate des Forschungsprogrammes KLIMUS und ihre Anwendung in der Raumplanung. – Geogr. Bernens., CH.

Mauder, M., R.L. Desjardins, Z. Gao, R. van Haarlem, 2008: Errors of Naturally Ventilated Air Temperature Measurements in a Spatial Observation Network. – J. Atmos. Ocean. Tech. **25**, 2145–2151. DOI:10.1175/2008JTECHA1046.1.

Meier, F., D. Fenner, T. Grassmann, M. Otto, D. Scherer, 2017: Crowdsourcing air temperature from citizen weather stations for urban climate research. – Urban Climate **19**, 170–191. DOI:10.1016/j.uclim.2017.01.006.

Melhuish, E., M. Pedder, 1998: Observing an urban heat island by bicycle. – Weather **53**, 121–128. DOI:10.1002/j.1477-8696.1998.tb03974.x.

MeteoSwiss, 2020: Climate Normals Bern/Zollikofen. – Federal Office of Meteorology and Climatology MeteoSwiss, Zurich.

Micronel, 2003: D480T / D480Q Axiallüfter. – https://www.micronel.com/uploads/tx_micronel/D480Q_mit_3-Litzen_Anschlusschema.pdf. (last access: 22 September 2021).

Muller, C.L., L. Chapman, C.S.B. Grimmond, D.T. Young, X. Cai, 2013: Sensors and the city: a review of urban meteorological networks: Sensors and the City. – Int. J. Climatol. **33**, 1585–1600. DOI:10.1002/joc.3678.

Muller, C.L., L. Chapman, S. Johnston, C. Kidd, S. Illingworth, G. Foody, A. Overeem, R.R. Leigh, 2015: Crowdsourcing for climate and atmospheric sciences: current status and future potential: Crowdsourcing for Climate and Atmospheric Sciences. – Int. J. Climatol. **35**, 3185–3203. DOI:10.1002/joc.4210.

Nakamura, R., L. Mahrt, 2005: Air Temperature Measurement Errors in Naturally Ventilated Radiation Shields. – J. Atmos. Ocean. Tech. **22**, 1046–1058. DOI:10.1175/JTECH1762.1.

Nakamura, Y., T.R. Oke, 1988: Wind, Temperature and Stability Conditions in an East-West Oriented Urban Canyon. – Atmos. Env. **22**, 2691–2700. DOI:10.1016/0004-6981(88)90437-4.

Napoly, A., T. Grassmann, F. Meier, D. Fenner, 2018: Development and Application of a Statistically-Based Quality Control for Crowdsourced Air Temperature Data. – Front. Earth Sci. **6**, 118. DOI:10.3389/feart.2018.00118.

Oke, T.R., 1976: The Distinction between Canopy and Boundary-layer Urban Heat Islands. – Atmosphere **14**, 268–77. DOI:10.1080/00046973.1976.9648422.

Oke, T.R., G. Mills, A. Christen, J.A. Voogt, 2017: Urban Climates. – Cambridge University Press, Cambridge. DOI:10.1017/9781139016476.

Onset Computer Corporation, 2018: HOBO® Pendant® Temperature Data Logger (UA-001-xx) Manual. – Onset Computer Corporation: https://www.onsetcomp.com/files/manual_pdfs/9531-O%20UA-001%20Manual.pdf (last access: 06 June 2021).

Rajkovich, N., L. Larsen, 2016: A Bicycle-Based Field Measurement System for the Study of Thermal Exposure in Cuyahoga County, Ohio, USA. – Int. J. Env. Res. Publ. Health **13**, 159. DOI:10.3390/ijerph13020159.

Robine, J.-M., S.L.K. Cheung, S. Le Roy, H. Van Oyen, C. Griffiths, J. -P. Michel, F.R. Herrmann, 2008: Death toll exceeded 70,000 in Europe during the summer of 2003. – Compt. Rend. Biol. **331**, 171–178. DOI:10.1016/j.crvi.2007.12.001.

Scherer, D., F. Ament, S. Emeis, U. Fehrenbach, B. Leitl, K. Scherber, C. Schneider, U. Vogt, 2019: Three-Dimensional Observation of Atmospheric Processes in Cities – Meteorol. Z. **28**, 121–38. DOI:10.1127/metz/2019/0911.

Sensirion The Sensor Company, 2014a: Sensirion Datasheet SHT20 Humidity and Temperature Sensor IC. – https://www.sensirion.com/fileadmin/user_upload/customers/sensirion/Dokumente/2_Humidity_Sensors/Datasheets/Sensirion_Humidity_Sensors_SHT20_Datasheet.pdf (last access: 06 June 2021).

Sensirion The Sensor Company, 2014b: Sensirion Datasheet SHT21 Humidity and Temperature Sensor IC. – https://www.sensirion.com/fileadmin/user_upload/customers/sensirion/Dokumente/2_Humidity_Sensors/Datasheets/Sensirion_Humidity_Sensors_SHT21_Datasheet.pdf (last access: 06 June 2021).

Sera, F., B. Armstrong, A. Tobias, A.M. Vicedo-Cabrera, C. Åström, M.L. Bell, B. -Y. Chen, M. de Sousa Zanotti Stagliorio Coelho, P. Matus Correa, J.C. Cruz, T.N. Dang, M. Hurtado-Diaz, D. Do Van, B. Forsberg, Y.L. Guo, Y. Guo, M. Hashizume, Y. Honda, C. Iñiguez, J.J.K. Jaakkola, H. Kan, H. Kim, E. Lavigne, P. Michelozzi, N.V. Ortega, S. Osorio, M. Pascal, M.S. Ragettli, N.R. I. Ryti, P.H. N. Saldiva, J. Schwartz, M. Scortichini, X. Seposo, S. Tong, A. Zanobetti, A. Gasparrini, 2019: How urban characteristics affect vulnerability to heat and cold: a multi-country analysis. – Int. J. Epidem. **48**, 1101–1112. DOI:10.1093/ije/dyz008.

Stewart, I.D., 2011: Redefining the Urban Heat Island. – Ph.D. thesis, University of British Columbia, Vancouver.

Stewart, I.D., T.R. Oke, 2012: Local Climate Zones for Urban Temperature Studies. – Bull. Amer. Meteor. Soc. **93**, 1879–1900. DOI:10.1175/BAMS-D-11-00019.1.

Sundborg, A. , 1951: Climatological Studies in Uppsala with Special Regard to the Temperature Conditions in the Urban Area. – Quart. J. Roy. Met. Soc. 78, 653–54. DOI:10.1002/qj.49707833828.

United Nations, 2019: World urbanization prospects: the 2018 revision. – United Nations, Department of Economic and Social Affairs, and Population Division, New York, ISBN: 978-92-1-148319-2.

Vicedo-Cabrera, A.M., N. Scovronick, F. Sera, D. Royé, R. Schneider, A. Tobias, C. Astrom, Y. Guo, Y. Honda, D.M. Hondula, R. Abrutzky, S. Tong, M. de Sousa Zanotti Stagliorio Coelho, P.H. Nascimento Saldiva, E. Lavigne, P. Matus Correa, N. Valdes Ortega, H. Kan, S. Osorio, J. Kyselý, A. Urban, H. Orru, E. Indermitte, J.J. K. Jaakkola, N. Ryti, M. Pascal, A. Schneider, K. Katsouyanni, E. Samoli, F. Mayvaneh, A. Entezari, P. Goodman, A. Zeka, P. Michelozzi, F. de'Donato, M. Hashizume, B. Alahmad, M. Hurtado Diaz, C. De La Cruz Valencia, A. Overcenco, D. Houthuijs, C. Ameling, S. Rao, F. Di Ruscio, G. Carrasco-Escobar, X. Seposo, S. Silva, J. Madureira, I.H. Holobaca, S. Fratianni, F. Acquaotta, H. Kim, W. Lee, C. Iniguez, B. Forsberg, M.S. Ragettli,

Y.L.L. Guo, B.Y. Chen, S. Li, B. Armstrong, A. Aleman, A. Zanobetti, J. Schwartz, T.N. Dang, D.V. Dung, N. Gillett, A. Haines, M. Mengel, V. Huber, A. Gasparrini, 2021: The burden of heat-related mortality attributable to recent human-induced climate change. – Nat. Climate Change **11**, 492–500. DOI:10.1038/s41558-021-01058-x.

Voogt, J.A., T.R. Oke, 2003: Thermal remote sensing of urban climates. – Rem. Sens. Env. 86, 370–384. DOI:10.1016/S0034-4257(03)00079-8.

White-Newsome, J.L., S.J. Brines, D.G. Brown, J.T. Dvonch, C.J. Gronlund, K. Zhang, E.M. Oswald, M.S. O'Neill, 2013: Validating Satellite-Derived Land Surface Temperature with in Situ Measurements: A Public Health Perspective. – Env. Health Persp. **121**, 925–931. DOI:10.1289/ehp.1206176.

WMO, 2006: Initial guidance to obtain representative meteorological observations at urban sites. Instruments and observing methods report No. 81. – World Meteorological Organization (WMO), Geneva.

Young, D.T., L. Chapman, C.L. Muller, X.-M. Cai, C.S.B. Grimmond, 2014: A Low-Cost Wireless Temperature Sensor: Evaluation for Use in Environmental Monitoring Applications. – J. Atmos. Ocean. Tech. **31**, 938–944. DOI:10.1175/JTECH-D-13-00217.1.

Zumwald, M., B. Knüsel, D.N. Bresch, R. Knutti, 2021: Mapping urban temperature using crowd-sensing data and machine learning. – Urban Climate **35**, 100739. DOI:10.1016/j.uclim.2020.100739.

The pdf version (Adobe Java Script must be enabled) of this paper includes an electronic supplement.